Accepted Manuscript

Serendipitous discovery of potent human head and neck squamous cell carcinoma anti-cancer molecules: A fortunate failure of a rational molecular design

Chiara Zagni, Venerando Pistarà, Luciana A. Oliveira, Rogerio M. Castilho, Giovanni Romeo, Ugo Chiacchio, Antonio Rescifina

PII: S0223-5234(17)30790-0

DOI: 10.1016/j.ejmech.2017.09.075

Reference: EJMECH 9790

To appear in: *European Journal of Medicinal Chemistry*

Received Date: 21 July 2017

Revised Date: 1 August 2017

Accepted Date: 29 September 2017

Please cite this article as: C. Zagni, V. Pistarà, L.A. Oliveira, R.M. Castilho, G. Romeo, U. Chiacchio, A. Rescifina, Serendipitous discovery of potent human head and neck squamous cell carcinoma anti-cancer molecules: A fortunate failure of a rational molecular design, *European Journal of Medicinal Chemistry* (2017), doi: 10.1016/j.ejmech.2017.09.075.

Serendipitous discovery of potent human head and neck squamous cell carcinoma anti-cancer molecules: A fortunate failure of a rational molecular design

Chiara Zagni [a, *], Venerando Pistarà [a], Luciana A. Oliveira [b], Rogerio M. Castilho [b], Giovanni Romeo [c], Ugo Chiacchio [a], Antonio Rescifina [a, *]

[a] Dipartimento di Scienze del Farmaco, Università degli Studi di Catania, V.le A. Doria, 95125 Catania, Italy.

[b] Laboratory of Epithelial Biology, Department of Periodontics and Oral Medicine, University of Michigan School of Dentistry, Ann Arbor, MI 48109-1078, USA.

[c] Dipartimento Farmaco-Chimico, Università di Messina, Viale SS. Annunziata, Messina 98168, Italy.

Corresponding authors:

Chiara Zagni chiarazagni@gmail.com; Antonio Rescifina arescifina@unict.it

Graphical Abstract

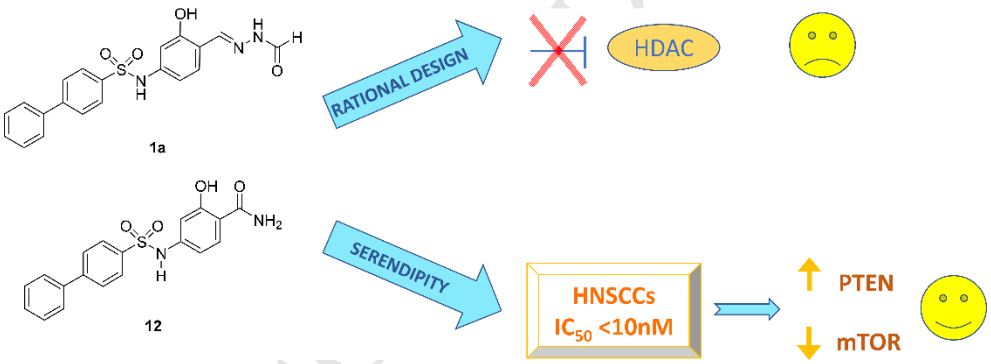

Highlights

- Novel anticancer molecules were designed and synthesized as HDAC inhibitors
- Compounds **1a** and **12** showed very low inhibitory activity over HDAC
- Compounds **1a** and **12** exhibited excellent anti-proliferative activity against HNSCCs
- Compounds **1a** and **12** enhanced PTEN expression
- Compounds **1a** and **12** were shown to block mTOR signaling

Keywords

HDAC; PTEN; HNSCC; PI3K/Akt/mTOR; Drug design; anti-cancer

Abstract

Histone deacetylase inhibitors (HDACis) play an important role as valuable drugs targeted to cancer therapy: several HDACis are currently being tested in clinical trials. Two new potential HDACis **1a** and **1d**, characterized by the presence of a biphenyl-4-sulfonamide group as a connection unit between the *N*-{4-[(*E*)-(2-formylhydrazinylidene)methyl]-3-hydroxyphenyl} and the 2-hydroxy-*N*-(trifluoroacetyl)benzamide moiety, respectively, as two zinc-binding group (ZBG), have been designed, synthesized and tested for their biological activity. Surprisingly, compounds **1a** and **12**, this last exclusively obtained in place of **1d**, exhibited a very low HDAC inhibitory activity. A serendipitous assay of these two compounds, conducted on three chemoresistant cell lines of head and neck squamous cell carcinoma (HNSCC), showed their antiproliferative activity at low nanomolar concentrations, better than cisplatin. In vitro, biological assays indicated that compounds **1a** and **12** are able to increase acetylation of histone H3 and to interfere with the PI3K/Akt/mTOR pathway by inducing the accumulation of PTEN protein.

1. Introduction

The epigenetic control of gene expression is operated through several post-translational modifications of chromatin such as methylation, acetylation, ubiquitination, phosphorylation, sumoylation. In particular, acetylation/deacetylation of ε-amino groups of lysine residues of histone tails plays a relevant role in cancer development [1, 2]. Histone acyl transferases (HATs) transfer an acetyl group from acetyl CoA to the amino group of the lysine residue to form ε-*N*-acetyl lysine. This modification neutralizes the positive charge of the lysine residues of histones, loosening their interactions with the negatively charged DNA and leading to an “open” chromatin structure that increases the binding of transcription factors, thus activating gene transcription [3]. Therefore, increased levels of histone acetylation are associated with enhanced transcriptional activity; conversely, decreased levels of acetylation are related to the repression of gene expression [4, 5].

HDACis selectively alters gene transcription by chromatin remodeling and the structure

modification of transcription complexes, triggering growth arrest, differentiation, activation of the extrinsic and/or intrinsic apoptotic pathways, cell death and senescence [6]. Histone deacetylase (HDAC) inhibitor activation of p21WAF1 involves changes in promoter-associated proteins, including HDAC1 [7]. Recent studies suggested that acetylation of non-histone proteins may also play an important role in biological effects of this class of compounds [8]. To date, more than 50 non-histone proteins with regulatory roles in cell proliferation, cell migration, and cell death have been identified as substrates of HDACis. For this reason, HDACis have recently emerged as an important target for therapeutic intervention in cancer and potentially other human diseases [9].

Epigenetic changes also play a key role in regulating gene expression through histone modifications. Inhibition of HDAC constitutes a novel strategy to disrupt the population of cancer stem cells in head and neck tumors and to create a homogeneous population of cancer cells with biologically defined signatures and predictable behavior [10].

Figure 1 reports the structure of some HDACis: SAHA (Zolinza®), Romidepsin (Istodax®), and Belinostat (PXD101) approved by FDA for the treatment of cutaneous T-cell lymphoma (CTCL), Panobinostat (LBH589, Faridak) licensed for the treatment of multiple myeloma [https://www.fda.gov], Chidamide [11] approved by the Chinese FDA for the treatment of CTCL and TSA.

To date, more than 20 inhibitors are under preclinical and clinical investigation as single agents and in combination therapies against different cancers. The most promising compounds in clinical trials include MGCD-0103 (Methylgene, phase II) [12] and MS-275 (Syndax, phase II) [https://clinicaltrials.gov] (Fig. 1).

Co-crystal structures of hydroxamate HDAC inhibitor Trichostatin A (TSA) with histone deacetylase homologue from the hyperthermophilic bacterium *Aquifex aeolicus* revealed an active site consisting of a tubular pocket, a zinc-binding site, and two Asp-His charge-relay systems, all of which are believed to be involved in the mechanism of HDAC inhibition [13]. All the classical HDACis (classes I, II, IV) require Zn^{2+} as a cofactor for their deacetylase activity [14]. HDACis

contain three key structural elements to their pharmacophore: a zinc-binding group (ZBG), which coordinates the zinc ion at the bottom of the long narrow active site cavity; a capping group, which interacts both with the amino acids on the rim of the binding cavity and the protein surface; a linker domain, whose role is to ensure the correct positioning of the two former groups and interact with the lipophilic binding tunnel [15].

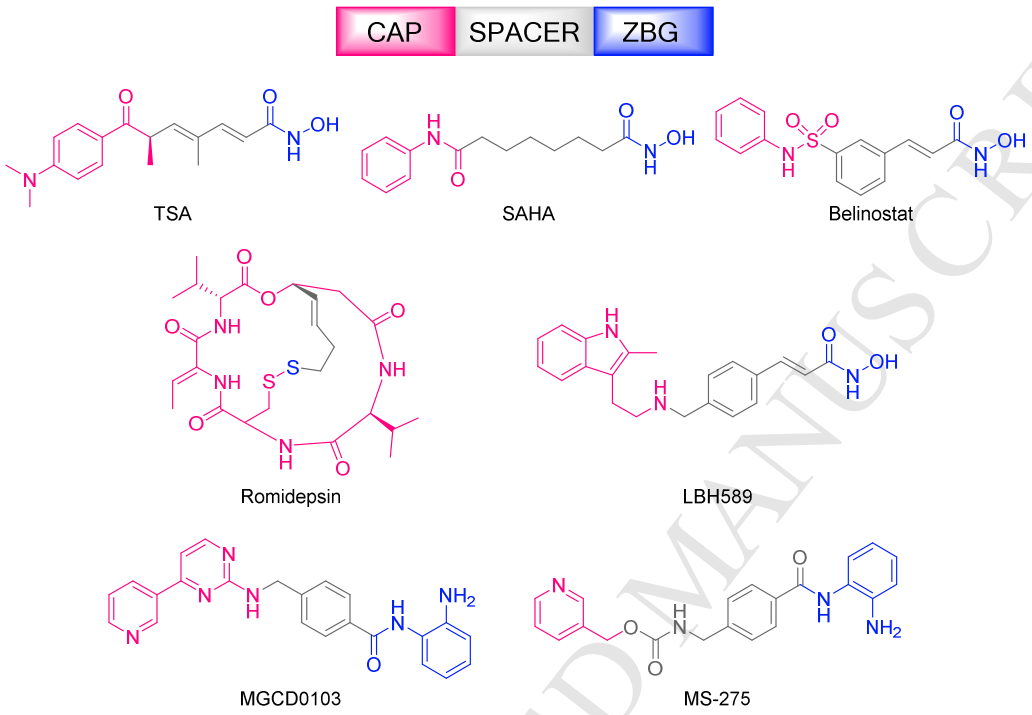

Fig. 1. Structures of some HDACis in clinical development or clinical use.

Following our recent interest in the research of more potent HDACis, we have designed and studied *in silico* four potential HDAC inhibitors. Based on molecular docking results, we decided to synthesize two of these molecules, the *N*-{4-[(*E*)-(2-formylhydrazinylidene)methyl]-3-hydroxyphenyl}biphenyl-4-sulfonamide (**1a**) and the 4-[(biphenyl-4-ylsulfonyl)amino]-2-hydroxy-*N*-(trifluoroacetyl)benzamide (**1d**); unfortunately, in place of this last we exclusively obtained the 4-[(biphenyl-4-ylsulfonyl)amino]-2-hydroxybenzamide (**12**). Compounds **1a** and **12**, contrary to *in silico* predictions, have shown a not appreciable HDAC activity. However, the synthesized compounds, serendipitously evaluated for their antiproliferative activity on three human head and neck squamous cell carcinoma (HNSCCs) cell lines (HN6, HN12, and HN13), exhibited an IC_{50} in

the low nanomolar range. To investigate the possible mechanism of action we performed a series of biological screenings. Considering that in a significant number of HNSCCs tumor progression results from mutations in genes, such as *PTEN* and *PIK3CA*, that causes alterations in cell signaling cascade PI3K/Akt/mTOR, resulting in aberrant cell growth, migration, and survival [16, 17], we performed western blot assays that highlighted that compounds **1a** and **12** cause a robust accumulation of the tumor suppressor PTEN, that acts as a negative regulator of the phosphatidylinositol 3-kinase (PI3K) pathway [18-21].

Despite the not encouraging obtained results on HDAC inhibition, because of compound **1a**, however, present a low activity, we conducted an immunohistochemistry assay in order to verify the effective acetylation of histones in the cells, on both compounds, for comparison. Surprisingly, the results indicated that the two molecules promote a dose dependent acetylation of histone H3 in HNSCCs. These results point out that the acetylation could occur *via* another mechanism.

2. Results and Discussion

2.1. Molecular drug design

Nowadays, the design of new HDACis is principally focused on changing the capping group and the linker domain given that the hydroxamic acid functionality is the best ZBG. We, on the search of new non-hydroxamates HDACis, designed four new ZBGs on the basis of the three-dimensional structure of the active site of the HDAC8 enzyme. In fact, with the exception of HDAC8, functional HDACis were found as high-molecular-weight multiprotein complexes, and most purified recombinant HDACis are enzymatically inactive [22]; therefore, HDAC8 is the best model among mammalian HDACis, if we look at it from a structural biology perspective. So, looking at the pose of TSA in the co-crystallized structure with the human HDAC8 (PDB ID: 1T64) and considering that hydroxamic acid group chelates the zinc ion in a bidentate fashion and forms hydrogen bonds with Tyr306 and Asp178 (Fig. 2A) we designed, as new ZBGs, a (2-formylhydrazinylidene)methyl (a), a [2-(trifluoroacetyl)hydrazinylidene]methyl (b), a (2-formylhydrazinyl)carbonyl (c), and a

(trifluoroacetyl)carbamoyl (d) moieties which could coordinate the zinc ion bi- or tridentately and could also form hydrogen bonds with Tyr306, Asp178, and, probably, with other amino acids at the bottom of the channel (Fig. 2B). Contemporarily, we choose as linker a *para* disubstituted benzene carrying in *ortho* to ZBG a hydroxyl functionality that, in principle, could be further involved in the zinc chelation. Finally, for the CAP we focused on the bifenilsulfonamide basing on an extensive QSAR modeling study of sulfonamide HDACis [23]. The new four molecules **1a**–**d** have been represented in Figure 2C.

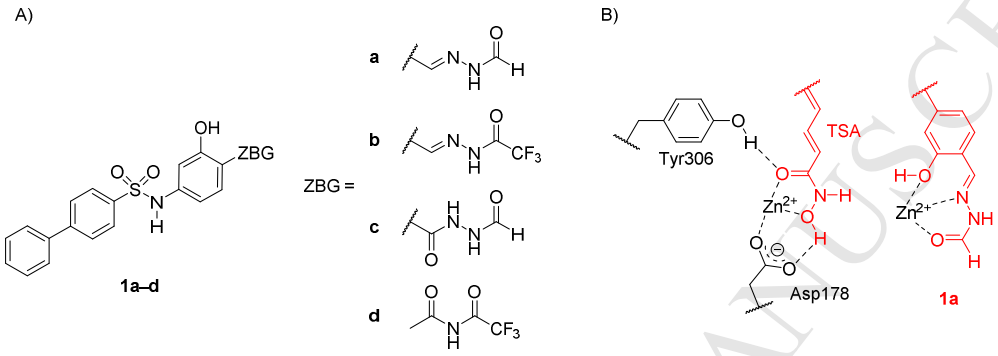

Fig. 2. A) Chemical structure of the new designed potential HDACis **1a**–**d**. B) Interactions of TSA in the co-crystallized structure with the human HDAC8 (PDB ID: 1T64) and proposed tridentate chelation of ZBG A with Zn^{2+}.

The molecular docking simulations of all new compounds showed that compound incorporating the A and D ZBG could be good candidates as HDACis with a ΔG_{bind} of –11.63 and –9.84 kcal/mol, respectively. These energy values are, for **1a**, better than that predicted for TSA (ΔG_{bind} = –11.13 kcal/mol) and SAHA (ΔG_{bind} = –10.03 kcal/mol), the two most famous HDACis, chosen as reference compounds (Table 1). The calculated K_i values for TSA and SAHA have been about 10-fold underestimated.

Table 1

Predicted K_i for the four designed compounds, TSA, and SAHA, and experimental K_i for the last two.

Compound	ΔG_{bind} (kcal/mol)	Calculated K_i (nM)	Experimental K_i (nM)
1a	–11.63	2.9	—[a]

1b	–8.78	363.8	—[b]
1c	–8.39	703.0	—[b]
1d	–9.84	60.7	—[c]
SAHA	–10.03	44.1	480[d]
TSA	–11.13	6.9	45[d]

[a] IC_{50} reported in section 2.3.1.
[b] Not synthetized.
[c] Not obtained.
[d] From reference [24].

The 3D and 2D sketch of the docked pose for the best scored compound **1a** (Fig. 3) highlight that this compound chelate the Zn^{2+} bidentately by the *o*-OH and the double bonded hydrazinic nitrogen atom, whereas an extended network of hydrogen bonds establish between carbonyl oxygen and His142 and Gln263, between NH and Asp178, and between *o*-OH and Tyr306, confirming the designed previsions.

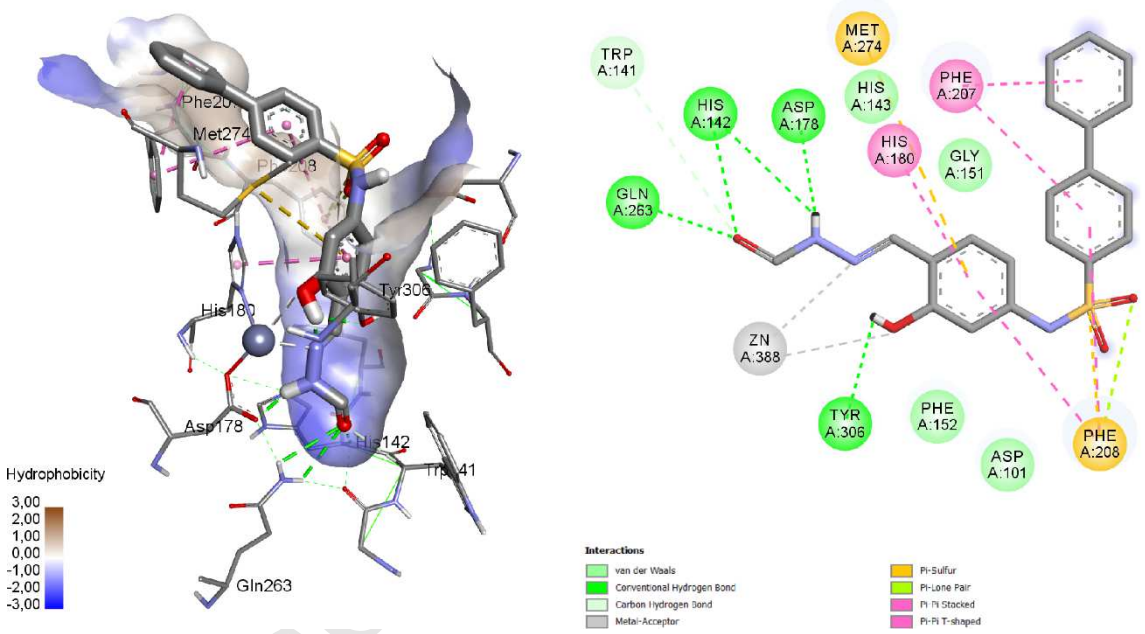

Fig. 3. 3D and 2D view of the interactions for **1a** inside the binding pocket of HDAC8 (PDB ID: 1T64).

2.2. Chemistry

Basing on the molecular modeling results, and considering the about 10-fold K_i underestimation, we choose to synthesize only compounds **1a** and **1d**. The synthetic route towards these two compounds is shown in Schemes 1 and 2. The first step of the synthesis involved the conversion of *p*-aminosalicylic acid **2** into the methyl ester **3** that reacted with diphenyl sulphonyl chloride in order

to obtain the correspondent sulfonamides **4** (Scheme 1). Compound **4** was subsequently protected at nitrogen and oxygen atoms by treatment with benzyl bromide providing compound **5**. The ester **5** was reduced by lithium aluminum hydride in THF anhydrous to benzyl alcohol **6**, successively oxidized with activated MnO_2 to give the aldehyde **7**. The reaction of compound **7** with formylhydrazine gives rise to compound **8** that was deprotected with catalytic hydrogenation to the target compound **1a**.

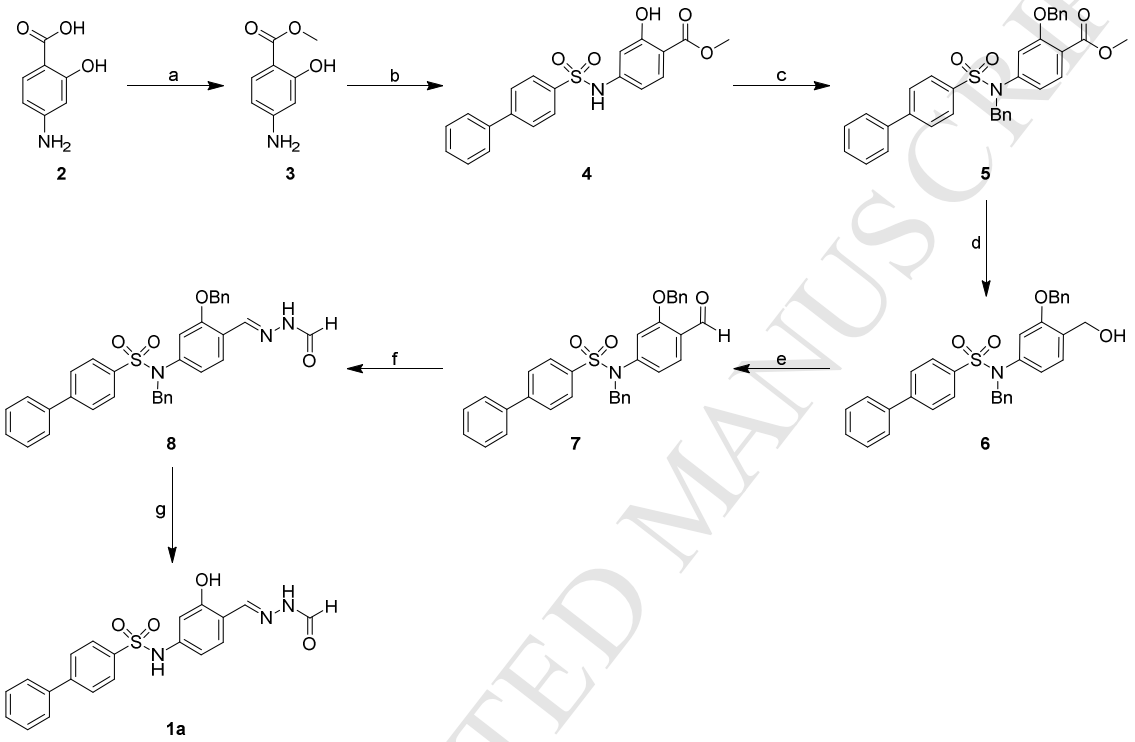

Scheme 1. Synthetic route to **1a**. Reagents and conditions: a) H_2SO_4, CH_3OH, reflux, 4 h; b) diphenylsulfonyl chloride, Py, THF, r.t., 12 h; c) K_2CO_3, BnBr, acetone, reflux, 12 h; d) $LiAlH_4$, THF, H_2O, –78 °C, 5 h; e) MnO_2, CH_2Cl_2, reflux, 12 h; f) formylhydrazine, EtOH, reflux, 12 h; g) H_2, Pd/C, MeOH, r.t., 12 h.

For the synthesis of **1d**, the ester **5** was hydrolyzed to acid **9** that was converted into the corresponding chloride **10** (Scheme 2), which in turn was treated with trifluoromethylacetamide. Unfortunately, this last step conducted to the amide **11** that was deprotected to afford compound **12**. All attempts to synthesize compound **1d** failed. All the reaction carried out on compound **10** with trifluoroacetamide at different conditions led to the amide derivative **11**. This is probably due to a high reactivity to the hydrolysis process.

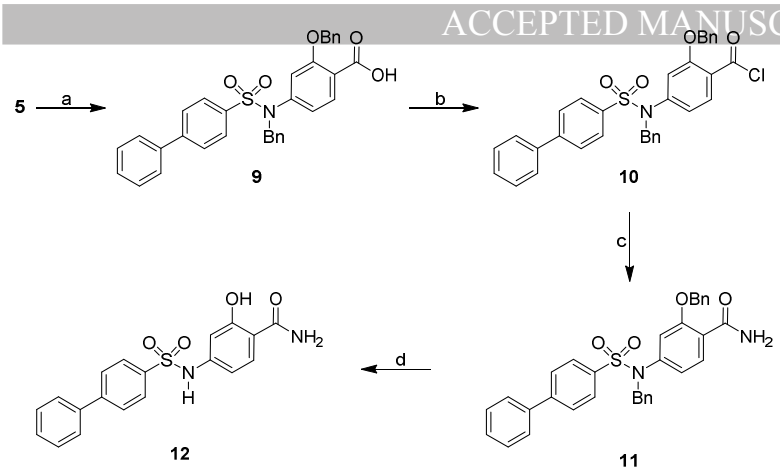

Scheme 2. The tentative synthetic route for **1d**. Reagents and conditions: (a) LiOH THF/MeOH, reflux 4 h; b) $SOCl_2$, reflux 10 h; c) Trifluoroacetamide, CH_3CN, overnight; d) H_2, Pd/C, MeOH, r.t., 12 h.

Compound **12**, docked into HDAC8, gave a predicted K_i of 716.8 nM (ΔG_{bind} = –8.38 kcal/mol). In fact, the $–CONH_2$ moiety, combined with the hydroxylic one present in *ortho* to the benzene scaffold, can be considered as a ZBG group, as suggested by the best obtained docked pose.

2.3. Biology

2.3.1. HDACis inhibition assay and acetylation of histone H3 in HNSCCs

The sulfonamides derivatives **1a** and **12** were tested for inhibition of HeLa nuclear HDACis using TSA as a reference. Surprisingly, compound **1a** evaluation revealed a scarce inhibition potency with an IC_{50} of 292 μM, so as the unwanted compound **12** lead to 20% of inhibition at 500 μM.

Since the molecular modeling studies showed a certain affinity of **1a** with HDAC, we evaluated the capacity of compound **1a** and **12** to influence the acetylation status of histone H3. To this purpose, the HN13 cells were treated with two different concentrations (1 and 10 nM) of **1a** and **12** for 24 h. The transcribed proteins, analyzed by a Western blot assay as described in material and method, showed a dose dependent increasing acetylation status of histone H3 (Fig. 4), with the maximum activity at the IC_{50} values. Consistently, Western blot analysis revealed that TSA alone, enhanced acetylation of histone H3 (lys9) in HN13 cells (data not shown). Notably, the compounds showed acetylation activity at concentration 10-fold lower than the IC_{50} values. Thus, our data suggest that **1a** and **12** might alter acetylation of H3 and cause cell death in HNSCCs through changes in gene

transcription.

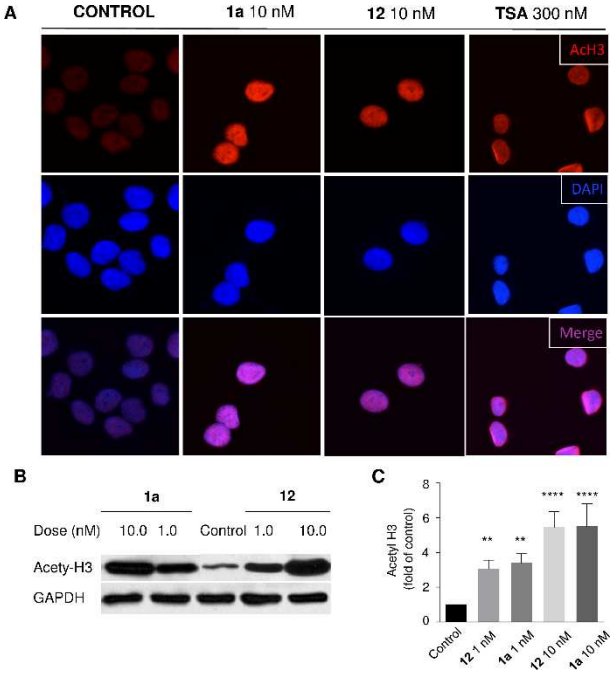

Fig. 4. A) Immunofluorescence images of Ac.H3 (lys9), DAPI staining and merge in untreated or treated HN13 cells with **1a**, **12**, and TSA as a positive control. B) Western blot for Ac. H3 (lys9) in HN13 cells in the presence or absence of **1a** and **12** at different concentrations. C) Quantification of acetyl H3 levels; **p < 0.01, ****p < 0.001.

2.3.2. Cell viability assay

Aiming at a preliminary screen for cellular activity, we tested the effect of compounds **1a** and **12** on the viability of three human head and neck squamous cell carcinoma (HNSCC) cell lines: HN6, HN12, and HN13.

Initially, the half-maximal inhibitory concentration (IC_{50}) was determined using the CellTiter 96TM Aqueous non-radioactive cell proliferation kit (Promega) according to manufacturer instructions. Interestingly, both compounds showed strong antiproliferative activities over all tested cell lines with IC_{50} in the range between 4.73 and 9.85 nM (Table 2, Fig. 5).

Table 2

In vitro efficacy assay of compounds **1a** and **12** on selected HNSCC cell lines and on non-cancer cells expressed as IC_{50}[a] (nM) at 24 h

Compound	HN6	HN12	HN13	184B5
1a	4.94 ±0.12	5.03 ±0.08	9.85 ±0.42	1840 ±125
12	4.73 ±0.34	4.99 ±0.19	9.66 ±0.34	1955 ±98

Cisplatin	16660[b]	30000[c]	41650[b]	25540[d]

[a] Mean of three independent triplicate experiments ± standard error.
[b] From reference [16].
[c] Value at 48 h. From reference [25].
[d] GI_{50} value at 48 h. From reference [26].

Moreover, the tested compounds showed better growth inhibition than cisplatin (>3300-fold), an established and effective treatment for HNSCC [27], at which these cell lines are particularly resistant. Finally, to determine if the newly synthesized compounds have differential cytotoxic effects on cancer and non-cancer cells, their cytotoxicity was also evaluated using 184B5 non-cancer immortalized breast epithelial cell lines. We found that the antiproliferative activity of compounds **1a** and **12** was not pronounced against the noncancer cell lines (Table 2) with a >186-fold and >200-fold selectivity, respectively, respect to the more resistant HN13 cancer cell lines.

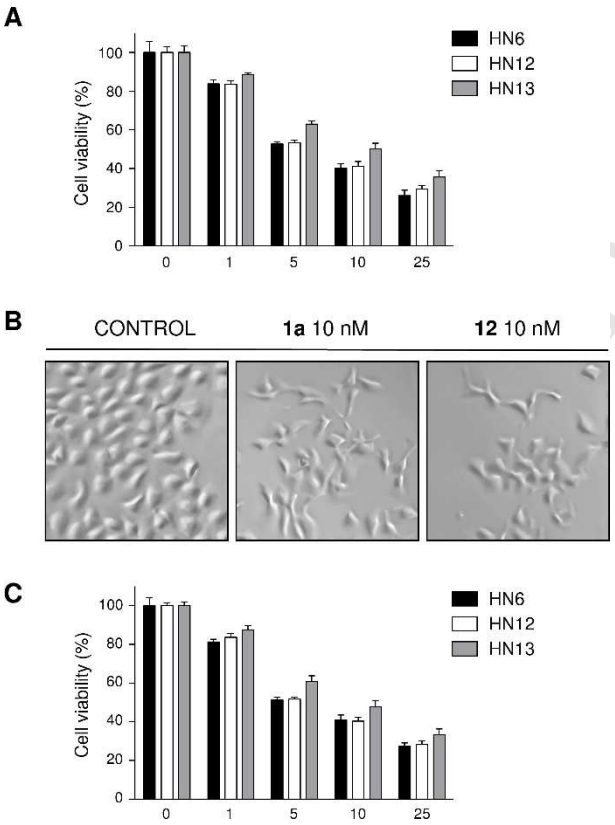

Fig. 5. Percentage of cell viability after 24 h of treatment with **1a** (A) and **12** (C). The concentration is expressed in nanomolar. B) Representation of HNSCC receiving vehicle, **1a** or **12** after 24 h.

2.3.3. Evaluation of PTEN

PTEN (phosphatase and tensin homolog deleted on chromosome ten) is one of the most frequently

mutated tumor suppressors in human cancer. PTEN functions through the regulation of the cell cycle, induction of tumor apoptosis, and inhibition of tumor cell growth, invasion and metastasis. Genetic analysis of PTEN in HNSCC has demonstrated alterations in PTEN, suggesting that PTEN may play a role in HNSCC tumorigenesis [28]. The PI3K/Akt/mTOR pathway has been shown to play an important role in cancer [29]. Therefore, molecules that increase PTEN expression are promising antitumoral drugs. On these bases, we further decided to evaluate if compounds **1a** and **12** would have any effect over the reactivation of tumor suppressor genes. Towards this goal, we decided to explore the activation status of phosphatase and tensin homolog (PTEN) at the protein level. Using two different concentrations of compounds **1a** and **12** (1.0 and 10.0 nM) we treated HNSCC cell lines for 24 h and compared them to vehicle treated controls. Interestingly, we observed that compounds **1a** and **12** induced the expression of PTEN in a dose dependent manner (Fig. 6), similar to that observed with histone H3. Moreover, administration of compounds **1a** and **12** resulted in a dose dependent reduction in the levels of pS6, a protein used to access the activations status of the PI3K/Akt/mTOR pathway. Our results are exciting once that they demonstrate the molecular mechanism by which compounds **1a** and **12** reduced cellular viability of HNSCC cancer cells.

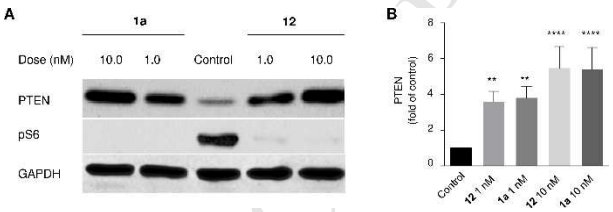

Fig. 6. A) Western blot of HNSCC cell line treated with compounds **1a** and **12** (1.0 and 10.0nM) for 24 h. Note the accumulation of PTEN upon and reduced activation of the PI3K/Akt/mTOR pathway evident by reduced accumulation of pS6, a marker for an active mTOR pathway. GAPDH served as a loading control. B) Quantification of PTEN levels; **p < 0.01, ****p < 0.001.

3. Conclusions

Two new molecules, *N*-{4-[(*E*)-(2-formylhydrazinylidene)methyl]-3-hydroxyphenyl}biphenyl-4-

sulfonamide (**1a**) and 4-[(biphenyl-4-ylsulfonyl)amino]-2-hydroxy-*N*-(trifluoroacetyl)benzamide (**1d**) have been designed and synthesized; unfortunately, in place of **1d** we exclusively obtained the 4-[(biphenyl-4-ylsulfonyl)amino]-2-hydroxybenzamide (**12**). Compounds **1a** and **12** were assayed, with negative results, as HDACis. Fortunately, these compounds were evaluated as antitumoral agents, exhibiting potent antiproliferative activities against HNSCCs cell lines with an IC_{50} in the low nanomolar range (4.73–9.85 nM). Both compounds are also able to increase the acetylation status of histone H3, a classical marker of HDAC inhibition. Finally, these two compounds interfere with PI3K/Akt/mTOR pathway by increasing PTEN expression and downregulate mTOR, as shown by western blot results.

With these results, we can speculate that the antitumoral activity exhibited by **1a** and **12** is due to a combined effect over histone H3 acetylation and PI3K/Akt/mTOR pathway.

Considering the significance of PTEN as a tumor suppressor gene and that germline mutations in PTEN are associated with several autosomal dominant hamartoma syndromes [20] including Cowden's disease, Bannayan-Riley-Ruvalcaba syndrome, and Lhermitte-Duclos syndrome, the importance of the results obtained with these two compounds deserve to be further deepened.

Moreover, also considering that HNSCC is the most frequent malignant tumor of the head and neck region and it is the sixth leading cancer by incidence worldwide, that the five-year survival rate of patients with HNSCC is about 40-50% [30], and that, despite advances in treatment, the mortality rate of patients treated with platinum-based chemotherapy has not changed markedly over the last few decades, due to chemoresistance [31], we have engaged further studies to better identify the antitumoral activity of these new compounds.

4. Experimental Section

4.1. In silico studies

4.1.1. Preparation of protein and ligands

The fully optimized crystal structure of the HDAC8/TSA complex (PDB ID: 1T64) was retrieved

from the PDB_REDO databank. The PDB_REDO procedure combines re-refinement and rebuilding within a unique decision-making framework to improve structures, using a variety of existing and custom-built software modules. This approach allows to choose an optimal refinement protocol (e.g. anisotropic, isotropic or overall B-factor refinement, TLS model) and to optimize the geometry versus data-refinement weights. Next, it proceeds to rebuild side chains and peptide planes before a final optimization round [32].

From the refined structure were retained only the A chain, one TSA molecule, and Zn^{2+} atom. Only for docking purpose, the 3D structure of the TSA was extracted from the PDB files whereas all other ligands were built using Gabedit (2.4.8) software [33] and all geometries were fully optimized, in the same software, with the semi-empirical PM6 [34] Hamiltonian implemented in MOPAC2016 (17.130W) [35].

4.1.2 Docking protocol

Macromolecule and ligands were prepared with Vega ZZ (3.1.1) [36] assigning Gasteiger charges to the protein and AM1BCC ones to the ligand. Fine docking was performed by applying the Lamarckian genetic algorithm (LGA) implemented in AutoDock 4.2.6 [37] in combination with a specialized potential describing the interactions of zinc-coordinating ligands, named $AutoDock4_{Zn}$ [38]. The ligand-centered maps were generated by the program AutoGrid (4.2.6) with a spacing of 0.375 Å and dimensions that encompass all atoms extending 5 Å from the surface of the ligand. All of the parameters were inserted at their default settings. In the docking tab, the macromolecule and ligand are selected, and GA parameters are set as ga_runs = 100, ga_pop_size = 150, ga_num_evals = 20000000, ga_num_generations = 27000, ga_elitism = 1, ga_mutation_rate = 0.02, ga_crossover_rate = 0.8, ga_crossover_mode = two points, ga_cauchy_alpha = 0.0, ga_cauchy_beta = 1.0, number of generations for picking worst individual = 10.

Because no water molecule is directly involved in complex stabilization they were not considered in the docking process. All protein amino acidic residues were kept rigid whereas all single bonds of

ligands were treated as full flexible.

4.2. Chemistry. General

Solvents and reagents were used as received from commercial sources. Melting points were determined with a Kofler apparatus and are reported uncorrected. Elemental analyses were performed with a Perkin–Elmer elemental analyzer. NMR spectra (^{1}H NMR recorded at 500 MHz, ^{13}C NMR recorded at 125 MHz) were obtained on Varian Instruments and are referenced in ppm relative to TMS or the solvent signal. Thin-layer chromatographic separations were performed on Merck silica gel 60-F254 pre coated aluminum plates. Flash chromatography was accomplished on Merck silica gel (200–400 mesh).

Analyses indicated by the symbols of the elements or functions were within 0.4% of the theoretical values.

All reagents were purchased from Aldrich Co. All solvents were dried according to literature methods.

4.2.1. Synthesis of methyl 4-([1,1'-biphenyl]-4-ylsulfonamido)-2-hydroxybenzoate (**4**)

To a solution of biphenyl-4-sulfonyl chloride (10.58 g, 41.86 mmol) in dry THF (100 mL) at 0 °C, compound **3** (7.00 g, 41.86 mmol) in dry THF (50 mL) and dry pyridine (16.94 mL, 5 eq.) was added dropwise. The reaction mixture was allowed to warm to room temperature, stirred overnight and the solvent was evaporated under reduced pressure. The residue was purified by flash chromatography (ethyl acetate/cyclohexane 30:70) to afford the desired product **4** (88% yield) as yellow sticky solid. ^{1}H NMR spectrum (CD_3COCD_3, 500 MHz): δ = 3.87 (s, 3H, CH_3), 6.80–6.87 (m, 2H, CH), 7.38–7.99 (m, 10H, CH), 10.81 (s, 1H, OH). ^{13}C NMR ($CDCl_3$, 125 MHz): 52.67, 106.63, 108.71, 110.73, 128.07, 128.51, 128.61, 129.42, 129.93, 132.11, 145.73, 146.59. HRMS (ESI) calcd. for $C_{20}H_{17}NO_5S$ $[M+H]^+$, 383.0827; found, 383.0825.

4.2.2. Synthesis of methyl 4-(N-benzyl-[1,1'-biphenyl]-4-ylsulfonamido)-2-(benzyloxy)benzoate (**5**)

Compound **4** (2.87 g, 7.48 mmol) was dissolved in acetone (100 mL) and mixed with K_2CO_3 (5.17 g, 37.42 mmol, 5 eq.). The mixture was stirred at room temperature for 15 minutes. Then benzyl bromide (4.45 mL, 5 eq) was added and the reaction was heated under reflux for 12 h and neutralized with 1 M solution of HCl. After concentration under reduced pressure, the residue was purified through flash column chromatography (ethyl acetate/cyclohexane 20:80) to give the desired product **5** (93% yield) as light grey solid foam. ^{1}H NMR spectrum ($CDCl_3$, 500 MHz): δ = 3.85 (s, 3H, CH_3), 4.73 (s, 2H, CH_2), 4.98 (s, 2H, CH_2), 6.60-7.70 (m, 22H, CH). ^{13}C NMR ($CDCl_3$, 125 MHz): 52.02, 54.31, 70.62, 114.87, 119.56, 119.74, 126.74, 127.27, 127.37, 127.50, 127.81, 128.16, 128.41, 128.46, 128.51, 128.62, 129.09, 131.98, 135.25, 136.21, 136.66, 139.01, 143.46, 145.84, 158.22, 165.99. HRMS (ESI) calcd. for $C_{34}H_{29}NO_5S$ $[M+H]^+$, 563.1766; found, 563.1762.

4.2.2. Synthesis of N-benzyl-N-(3-(benzyloxy)-4-(hydroxymethyl)phenyl)-[1,1'-biphenyl]-4-sulfonamide (**6**)

A solution of ester **5** (1.75 g, 3.10 mmol) in THF (60 mL) at –78 °C was treated with $LiAlH_4$ (0.35 g, 9.31 mmol, 3 eq.). The reaction mixture was stirred at –78 °C until completion (generally 6 h) as determined by TLC. The cooling bath was then removed, and the reaction mixture was quenched with a 1 M solution of HCl followed by extraction of the aqueous layer with ethyl acetate. The combined organic layers were washed with water and brine, dried over Na_2SO_4, and concentrated in vacuum. The combined organic layers were washed with water and brine, dried with Na_2SO_4, and concentrated in vacuum. Chromatography on silica gel with ethyl acetate/cyclohexane 30:70 as the eluent afforded the targeted alcohol **6** (yield 71%) as light yellow sticky solid. ^{1}H NMR spectrum ($CDCl_3$, 500 MHz): δ = 4.62 (s, 2H, CH_2), 4.72 (s, 2H, CH_2), 4.89 (s, 2H, CH_2), 6.52-7.74 (m, 22H, CH). ^{13}C NMR ($CDCl_3$, 125 MHz): 54.88, 61.43, 70.17, 113.65, 120.36, 127.28, 127.40, 127.67, 128.14, 128.27, 128.37, 128.41, 128.55, 128.65, 129.08, 129.29, 135.75, 136.21, 137.07, 139.15, 139.36, 145.60, 156.33. HRMS (ESI) calcd. for $C_{33}H_{28}N_2O_4S$ $[M+H]^+$, 536.1896; found, 536.1900.

4.2.3. Synthesis of N-benzyl-N-(3-(benzyloxy)-4-formylphenyl)-[1,1'-biphenyl]-4-sulfonamide (**7**)

The alcohol **6** (0.87 g, 1.63 mmol) was stirred with anhydrous CH_2Cl_2 (50 mL) and heated slowly until reflux. Activated MnO_2 (1.42 g, 16.0 mmol, 10 eq.) was added in small portions over 15 min. Reflux was maintained for 10h after which the reaction was monitored by TLC. The reaction mixture was cooled to room temperature and filtered through celite using CH_2Cl_2 for washings. The yellow filtrate was concentrated under vacuum a purified by flash column chromatography (ethyl acetate/cyclohexane 10:90) to raise the aldehyde **7** (63% yield) as yellow solid foam. ^{1}H NMR spectrum ($CDCl_3$, 500 MHz): δ = 4.77 (s, 2H, CH_2), 5.03 (s, 2H, CH_2), 6.62-7.70 (m, 22H, CH), 10.40 (s, 1H, CHO). ^{13}C NMR ($CDCl_3$, 125 MHz): 54.14, 70.69, 114.48, 119.32, 124.04, 127.30, 127.35, 127.60, 127.89, 128.12, 128.38, 128.55, 128.73, 129.13, 135.18, 135.58, 136.60, 138.98, 145.69, 146.03, 160.93, 188.77. Anal. HRMS (ESI) calcd. for $C_{33}H_{28}N_2O_4S$ $[M+H]^+$, 534.1739; found, 534.1735.

4.2.4. Synthesis of (N-benzyl-N-(3-(benzyloxy)-4-((2-formylhydrazono)methyl)phenyl)-[1,1'-biphenyl]-4-sulfonamide (**8**)

Aldehyde **7** (0.20 g, 0.37 mmol) was heated in boiling EtOH (20 mL) until complete dissolution. *N*-formyl hydrazine (0.07 g, 1.12 mmol, 3 eq.) was added portionwise and the reaction maintained under reflux for 12 h. The mixture was then extracted with ethyl acetate, washed with brine, dried over Na_2SO_4, and concentrated in vacuum. Chromatography on silica gel, using a gradient of ethyl acetate/cyclohexane and 0.1% of triethylamine as eluent, gave product **8** (79% yield) as light yellow sticky solid. ^{1}H NMR ($CDCl_3$, 500 MHz): δ = 4.75 (s, 2H, CH), 4.93 (s, 2H, CH), 6.58-8.15 (m, 23H, CH), 8.72 (d, 1H, CHO), 9.28 (bs, 1H, NH). ^{13}C NMR ($CDCl_3$, 125 MHz): 61.44, 70.17, 113.66, 120.37, 127.29, 127.41, 127.67, 127.49, 128.15, 128.28, 128.38, 128.42, 128.55, 128.66, 129.01, 129.30, 135.76, 136.22, 137.08, 139.16, 139.35, 145.61, 156.34. HRMS (ESI) calcd. for $C_{33}H_{28}N_2O_4S$ $[M+H]^+$, 576.1957; found, 576.1951.

4.2.5. Synthesis of N-{4-[(E)-(2-formylhydrazinylidene)methyl]-3-hydroxyphenyl}biphenyl-4-sulfonamide (**1a**)

Pd/C (10%, 0.2 equiv) was added to a solution of **8** (0.5 g, 0.87 mmol) in ethyl acetate (10 mL). The mixture was refluxed under hydrogen at atmospheric pressure. After consumption of the required volume of hydrogen, the mixture was filtered on Celite, and the filtrate was concentrated under reduced pressure. The solid was purified by column chromatography (ethyl acetate/cyclohexane 40:60) (81% yeld) as pale yellow solid; m.p. 243–244 °C. ^{1}H NMR (CD_3COCD_3, 500 MHz): δ = 6.84–8.18 (m, 13 H), 8.36 (s, 1H, *syn*-CHO), 8.74 (s, 1H, *anti*-CHO), 9.42 (bs, 1H, NH), 10.34 (bs, NH), 10.67 (bs, 1H, CHO), 11.42 (bs, 1H, OH). ^{13}C NMR (CD_3COCD_3, 125 MHz): 107.65, 111.23, 111.63, 114.89, 115.26, 128.06, 128.39, 128.41, 128.60, 129.38, 129.40, 129.94, 132.38, 132.92, 139.57, 139.85, 141.72, 142.03, 146.33, 147.85, 150.63, 157.15, 159.17, 164.40. HRMS (ESI) calcd. for $C_{20}H_{18}N_3O_4S$ $[M+H]^+$, 396.1018; found, 396.1021.

4.2.6. Synthesis of 4-[benzyl(biphenyl-4-ylsulfonyl)amino]-2-(benzyloxy)benzoic acid (**9**)

To a solution of ester **5** (2.46 g, 4.36 mmol) in a THF/H_2O mixture (1:1, 50 mL) LiOH (0.52 g, 21.82 mmol, 5 eq.) was added. The reaction proceed under reflux for 24 h. The reaction mixture was netraulized with a 6M solution of HCl and extracted with EtOAc. The combined organic layer was collected, dried over anhydrous Na_2SO_4 and concentrated under reduced pressure to give a white residue, which was purified by silica gel chromatography (EtOAc: Hexane, 30:70) to give **9** as off white solid foam in 76% yield. ^{1}H NMR ($CDCl_3$, 500 MHz): δ = 4.82 (d, 2H, CH_2), 4.99 (d, 2H, CH_2), 6.79-7.94 (m, 22H, CH), 12.68 (s, 1H, OH). ^{13}C NMR ($CDCl_3$, 125 MHz): 54.03, 72.17, 114.83, 117.29, 119.91, 127.25, 127.62, 127.81, 127.92, 128.04, 128.34, 128.56, 128.67, 129.00, 129.01, 133.69, 134.19, 134.97, 136.35, 139.35, 144.72, 146.09, 157.39, 165.12. HRMS (ESI) calcd. for $C_{33}H_{28}NO_5S$ $[M+H]^+$, 550.1688; found, 550.1691.

4.2.7. Synthesis of 4-[benzyl(biphenyl-4-ylsulfonyl)amino]-2-(benzyloxy)benzoyl chloride (**10**)

To the acid **9** (0.85 g, 1.55 mmol) $SOCl_2$ (8 mL) was added. The reaction was refluxed for 4 h after which the excess thionyl chloride was removed under vacuum and the product was used without further purification.

4.2.8. Synthesis of 4-[benzyl(biphenyl-4-ylsulfonyl)amino]-2-(benzyloxy)benzamide (**11**)

To chloride **10** (0.60 g, 1,06 mmol), in CH_3CN (30 mL), trifluoracetamide (0.18 g, 1.59 mmol, 1,5 eq.) was added. The reaction was conducted for 12 h. Finally, the product was purified by flash chromatography (EtOAc/Hexane, 40:60) to give **11** (64% yield) as white sticky solid. ^{1}H NMR ($CDCl_3$, 500 MHz): δ = 4.77 (s, 2H, CH_2), 5.03 (s, 2H, CH_2), 5.63 (bs, 2H, NH_2) 6.61-8.05 (m, 22 H, CH). ^{13}C NMR ($CDCl_3$, 125 MHz): 52.02, 72.39, 114.86, 117.08, 119.95, 126.33, 127.28, 127.65, 127.95, 128.06, 128.24, 128.37, 128.60, 128.72, 129.12, 133.88, 133.97, 135.00, 136.35, 138.88, 144.88, 146.13, 157.27, 164.73. HRMS (ESI) calcd. for $C_{33}H_{28}N_2O_4S$ $[M+H]^+$, 548.1770; found, 548.1775.

4.2.9. Synthesis of 4-[(biphenyl-4-ylsulfonyl)amino]-2-hydroxybenzamide (**12**)

Pd/C (0.04 g, 0.338 mmol) was added to a solution of **11** (0.2 g, 0.36 mmol) in ethyl acetate (10 mL). The mixture was refluxed under hydrogen at atmospheric pressure. After consumption of the required volume of hydrogen, the mixture was filtered on Celite, and the filtrate was concentrated under reduced pressure. The solid was purified by column chromatography (ethyl acetate/cyclohexane 40:60) to give **12** (80% yield) as white solid; m.p. 285–286 °C. ^{1}H NMR (CD_3COCD_3, 500 MHz): δ = 6.78–7.89 (m, 12 H), 7.22 (bs, 2H, NH_2), 9.45 (bs, 1H, NH), 13.11 (s, 1H, OH). ^{13}C NMR (CD_3COCD_3, 125 MHz): 107.67, 109.99, 110.62, 110.89, 128.08, 128.47, 128.59, 129.41, 129.60, 129.63, 129.94, 139.54, 139.85, 144.30, 146.43, 164.32, 173.38. HRMS (ESI) calcd. for $C_{19}H_{17}N_2O_4S$ $[M+H]^+$, 369.0909; found, 369.0904.

4.3. Biological Evaluation

4.3.1. Measurement of HDAC Activity against HeLa Cell Nuclear Extract

HDAC inhibition was measured by a HDAC fluorometric drug screening kit procured from Biovision (catalog number K340-100). The kit was used according to the manufacturer's guidelines. The candidate compounds, assay buffer, and HDAC fluorometric substrate, which comprises an acetylated lysine side chain, were added to HeLa nuclear extracts in a 96-well plate and incubated at 37 °C for 60 min. The reaction was stopped by adding lysine developer, and the

mixture was incubated for another 30 min at 37 °C. An additional positive control included incubation with double-distilled water, and the inhibitor control consisted of incubation with Trichostatin A (TSA) at 20 μM. HDAC activities were quantified by a fluorescence plate reader with excitation at 370 nm and emission at 450 nm. The data analysis was performed using GraphPad Prism 6.0.

4.3.2. Cell Lines and Cell Culture

For cell culture experiments, human head and neck squamous cell carcinoma (HNSCCs) were obtained from University of Michigan (Ann Arbor, Michigan) All cancer cell lines were grown at 37 °C under humidified air supplemented with 5% CO_2 in DMEM containing 10% fetal calf serum, 120 μg/mL streptomycin. The cells were grown to 70–80% confluence before using them for the appropriate assays.

4.3.3. MTT Cell Viability Assay

The rate of cell survival under the action of test substances was evaluated by an improved MTT assay as previously described.[39] The assay is based on the ability of viable cells to metabolize yellow 3-(4,5-dimethylthiazol-2-yl)-2,5-diphenyltetrazolium bromide (MTT, Applichem,) to violet formazan that be detected spectrophotometrically. In brief, HN6, HN12, and HN13 cell lines were seeded in 96-well plates (Corning, USA). After 24 h, cells were exposed to increased concentrations of the test compounds. Incubation was ended after additional 24 h, and cell survival was determined by addition of MTT solution (5 mg/mL in phosphate buffered saline). The formazan precipitate was dissolved in DMSO (VWR, USA). Absorbance was measured at 590 nm in an FLUOstar microplate reader (BMG LabTech).

4.3.4. Western Blot

HN13 cells were treated with compounds **1a** and **12** and lysed with lysis buffer containing 0.2 M

Tris pH 7.5, SDS 20%, 14.3 M 2-betamercaptoetanol and protease inhibitors at 4 °C, and the supernatant was obtained after centrifuged at 16000 rpm, 4 °C for 10 min. A BCA protein assay reagent kit (Beyotime Institute of Biotechnology) was used to quantify the protein concentration. Identical amounts of protein from each sample (30 μg) were applied for SDS-PAGE and then transferred to the polyvinylidene difluoride membrane (Millipore, USA). The membranes were blocked for 1h at room temperature with 5% milk and incubated with PTEN (Cell Signaling Technology, 9559), Antiacetyl-Histon H3 (Cell Signaling, USA) and GAPDH (EMD Millipore, CB1001) primary antibodies. Membranes were then incubated with the IgG-HRP conjugated secondary antibody, and immunoblots were developed using a chemiluminescent-HRP substrate.

4.3.5. Immunofluorescence

HN13 were seeded onto glass coverslips, incubated at 37 °C overnight and treated with compounds **1a** and **12** for 24 h. The cells were then fixed with 4% paraformaldehyde, permeabilized with 0.5% Triton X-100, washed with PBS and blocked with 3% bovine serum albumin (BSA)/PBS. Samples were incubated in anti-AcH3 primary antibody (Cell Signaling, USA) for 2 h, followed by incubation with TRITC-conjugated anti-rabbit (Santa Cruz, USA) for 1 h. The samples were then stained with Hoechst 33342 (Invitrogen, H357C) diluted to 1: 5000 in H_2O. Coverslips were mounted in Fluoroshield (Sigma, USA**)** mounting medium. Images were taken using a QImaging ExiAqua monochrome digital camera attached to a Nikon Eclipse 80i Microscope (Nikon, Melville, NY) and visualized with QCapturePro software.

Appendix A. Supplementary data

Supplementary data related to this article can be found at http://dx.doi.org/

References

[1] G. Legube, D. Trouche, Regulating histone acetyltransferases and deacetylases, EMBO Rep., 4

(2003) 944-947.

[2] A.J. Bannister, T. Kouzarides, Regulation of chromatin by histone modifications, Cell Res., 21 (2011) 381-395.

[3] P.A. Marks, R.A. Rifkind, V.M. Richon, R. Breslow, T. Miller, W.K. Kelly, Histone deacetylases and cancer: causes and therapies, Nat. Rev. Cancer, 1 (2001) 194-202.

[4] J.E. Bolden, M.J. Peart, R.W. Johnstone, Anticancer activities of histone deacetylase inhibitors, Nat. Rev. Drug Discov., 5 (2006) 769-784.

[5] J. Deckert, K. Struhl, Histone Acetylation at Promoters Is Differentially Affected by Specific Activators and Repressors, Mol. Cell. Biol., 21 (2001) 2726-2735.

[6] C.Y. Gui, L. Ngo, W.S. Xu, V.M. Richon, P.A. Marks, Histone deacetylase (HDAC) inhibitor activation of p21WAF1 involves changes in promoter-associated proteins, including HDAC1, Proc. Natl. Acad. Sci. U. S. A., 101 (2004) 1241-1246.

[7] V.M. Richon, T.W. Sandhoff, R.A. Rifkind, P.A. Marks, Histone deacetylase inhibitor selectively induces p21WAF1 expression and gene-associated histone acetylation, Proc. Natl. Acad. Sci. U. S. A., 97 (2000) 10014-10019.

[8] W.S. Xu, R.B. Parmigiani, P.A. Marks, Histone deacetylase inhibitors: molecular mechanisms of action, Oncogene, 26 (2007) 5541-5552.

[9] R.R. Rosato, S. Grant, Histone deacetylase inhibitors: insights into mechanisms of lethality, Expert Opin. Ther. Targets, 9 (2005) 809-824.

[10] F.S. Giudice, D.S.P. Jr, J.E. Nör, C.H. Squarize, R.M. Castilho, Inhibition of Histone Deacetylase Impacts Cancer Stem Cells and Induces Epithelial-Mesenchyme Transition of Head and Neck Cancer, PLoS One, 8 (2013) e58672.

[11] Y. Shi, B. Jia, W. Xu, W. Li, T. Liu, P. Liu, W. Zhao, H. Zhang, X. Sun, H. Yang, X. Zhang, J. Jin, Z. Jin, Z. Li, L. Qiu, M. Dong, X. Huang, Y. Luo, X. Wang, X. Wang, J. Wu, J. Xu, P. Yi, J. Zhou, H. He, L. Liu, J. Shen, X. Tang, J. Wang, J. Yang, Q. Zeng, Z. Zhang, Z. Cai, X. Chen, K. Ding, M. Hou, H. Huang, X. Li, R. Liang, Q. Liu, Y. Song, H. Su, Y. Gao, L. Liu, J.

Luo, L. Su, Z. Sun, H. Tan, H. Wang, J. Wang, S. Wang, H. Zhang, X. Zhang, D. Zhou, O. Bai, G. Wu, L. Zhang, Y. Zhang, Chidamide in relapsed or refractory peripheral T cell lymphoma: a multicenter real-world study in China, J. Hematol. Oncol., 10 (2017) 69.

[12] N. Zhou, O. Moradei, S. Raeppel, S. Leit, S. Frechette, F. Gaudette, I. Paquin, N. Bernstein, G. Bouchain, A. Vaisburg, Z. Jin, J. Gillespie, J. Wang, M. Fournel, P.T. Yan, M.-C. Trachy-Bourget, A. Kalita, A. Lu, J. Rahil, A.R. MacLeod, Z. Li, J.M. Besterman, D. Delorme, Discovery of N-(2-aminophenyl)-4-[(4-pyridin-3-ylpyrimidin-2-ylamino)methyl]benzamide (MGCD0103), an orally active histone deacetylase inhibitor, J. Med. Chem., 51 (2008) 4072-4075.

[13] M.S. Finnin, J.R. Donigian, A. Cohen, V.M. Richon, R.A. Rifkind, P.A. Marks, R. Breslow, N.P. Pavletich, Structures of a histone deacetylase homologue bound to the TSA and SAHA inhibitors, Nature, 401 (1999) 188-193.

[14] M. Haberland, R.L. Montgomery, E.N. Olson, The many roles of histone deacetylases in development and physiology: implications for disease and therapy, Nat. Rev. Genet., 10 (2009) 32-42.

[15] A. Vannini, C. Volpari, G. Filocamo, E.C. Casavola, M. Brunetti, D. Renzoni, P. Chakravarty, C. Paolini, R. De Francesco, P. Gallinari, C. Steinkühler, S. Di Marco, Crystal structure of a eukaryotic zinc-dependent histone deacetylase, human HDAC8, complexed with a hydroxamic acid inhibitor, Proc. Natl. Acad. Sci. U. S. A., 101 (2004) 15064-15069.

[16] L.O. Almeida, A.C. Abrahao, L.K. Rosselli-Murai, F.S. Giudice, C. Zagni, A.M. Leopoldino, C.H. Squarize, R.M. Castilho, NFκB mediates cisplatin resistance through histone modifications in head and neck squamous cell carcinoma (HNSCC), FEBS open bio, 4 (2014) 96-104.

[17] J.M. Le, C.H. Squarize, R.M. Castilho, Histone modifications: Targeting head and neck cancer stem cells, World Journal of Stem Cells, 6 (2014) 511-525.

[18] T. Maehama, J.E. Dixon, The tumor suppressor, PTEN/MMAC1, dephosphorylates the lipid

second messenger, phosphatidylinositol 3,4,5-trisphosphate, The Journal of Biological Chemistry, 273 (1998) 13375-13378.

[19] V. Stambolic, A. Suzuki, J.L. de la Pompa, G.M. Brothers, C. Mirtsos, T. Sasaki, J. Ruland, J.M. Penninger, D.P. Siderovski, T.W. Mak, Negative regulation of PKB/Akt-dependent cell survival by the tumor suppressor PTEN, Cell, 95 (1998) 29-39.

[20] C. Eng, PTEN: one gene, many syndromes, Hum. Mutat., 22 (2003) 183-198.

[21] T. Maehama, PTEN: its deregulation and tumorigenesis, Biol. Pharm. Bull., 30 (2007) 1624-1627.

[22] N. Sengupta, E. Seto, Regulation of histone deacetylase activities, J. Cell. Biochem., 93 (2004) 57-67.

[23] D. Jaiswal, C. Karthikeyan, S.K. Shrivastava, P. Trivedi, QSAR modeling of sulfonamide inhibitors of histone deacetylase, Internet Electron. J. Mol. Des., 5 (2006) 345-354.

[24] J.E. Bradner, N. West, M.L. Grachan, E.F. Greenberg, S.J. Haggarty, T. Warnow, R. Mazitschek, Chemical phylogenetics of histone deacetylases, Nat. Chem. Biol., 6 (2010) 238-243.

[25] H.A. Sansing, A. Sarkeshik, J.R. Yates, V. Patel, J.S. Gutkind, K.M. Yamada, A.L. Berrier, Integrin alpha beta 1, alpha(v)beta, alpha(6)beta effectors p130Cas, Src and talin regulate carcinoma invasion and chemoresistance, Biochem. Biophys. Res. Commun., 406 (2011) 171-176.

[26] K. Patel, C. Karthikeyan, V.R. Solomon, N.S.H.N. Moorthy, H. Lee, K. Sahu, G.S. Deora, P. Trivedi, Synthesis of Some Coumarinyl Chalcones and their Antiproliferative Activity Against Breast Cancer Cell Lines, Lett. Drug Des. Discovery, 8 (2011) 308-311.

[27] K.P. Pendleton, J.R. Grandis, Cisplatin-Based Chemotherapy Options for Recurrent and/or Metastatic Squamous Cell Cancer of the Head and Neck, Clinical Medicine Insights: Therapeutics, 5 (2013) 103-116.

[28] L. L.-X., J.-X. Wu, W. Huang, The Prognostic Function of Biomarkers in Head and Neck

Squamous Cell Carcinomas HNSCC, Cancer Biology, 1 (2011) 51-60.

[29] D.A. Altomare, J.R. Testa, Perturbations of the AKT signaling pathway in human cancer, Oncogene, 24 (2005) 7455-7464.

[30] C.R. Leemans, B.J.M. Braakhuis, R.H. Brakenhoff, The molecular biology of head and neck cancer, Nat. Rev. Cancer, 11 (2011) 9-22.

[31] K.A.R. Price, E.E. Cohen, Current treatment options for metastatic head and neck cancer, Curr. Treat. Options Oncol., 13 (2012) 35-46.

[32] R.P. Joosten, K. Joosten, G.N. Murshudov, A. Perrakis, PDB_REDO: constructive validation, more than just looking for errors, Acta Crystallogr. D, 68 (2012) 484-496.

[33] A.R. Allouche, Gabedit-A Graphical User Interface for Computational Chemistry Softwares, J. Comput. Chem., 32 (2011) 174-182.

[34] J.J.P. Stewart, Optimization of parameters for semiempirical methods V: Modification of NDDO approximations and application to 70 elements, J. Mol. Mod., 13 (2007) 1173-1213.

[35] J.J.P. Stewart, MOPAC2016, in, Stewart Computational Chemistry, Colorado Springs, CO, USA, 2016.

[36] A. Pedretti, L. Villa, G. Vistoli, VEGA - An open platform to develop chemo-bio-informatics applications, using plug-in architecture and script programming, J. Comput. Aided Mol. Des., 18 (2004) 167-173.

[37] G.M. Morris, R. Huey, W. Lindstrom, M.F. Sanner, R.K. Belew, D.S. Goodsell, A.J. Olson, AutoDock4 and AutoDockTools4: Automated Docking with Selective Receptor Flexibility, J. Comput. Chem., 30 (2009) 2785-2791.

[38] D. Santos-Martins, S. Forli, M.J. Ramos, A.J. Olson, AutoDock4(Zn): an improved AutoDock force field for small-molecule docking to zinc metalloproteins, J. Chem. Inf. Model., 54 (2014) 2371-2379.

[39] H. Mueller, M.U. Kassack, M. Wiese, Comparison of the usefulness of the MTT, ATP, and calcein assays to predict the potency of cytotoxic agents in various human cancer cell lines, J.

Biomol. Screen., 9 (2004) 506-515.

The changes have been marked in yellow

Please, arrange the paragraph 2.1 as follow:

2.1. Molecular drug design

Nowadays, the design of new HDACis is principally focused on changing the capping group and the linker domain given that the hydroxamic acid functionality is the best ZBG. We, on the search of new non-hydroxamates HDACis, designed four new ZBGs on the basis of the three-dimensional structure of the active site of the HDAC8 enzyme. In fact, with the exception of HDAC8, functional HDACis were found as high-molecular-weight multiprotein complexes, and most purified recombinant HDACis are enzymatically inactive [22]; therefore, HDAC8 is the best model among mammalian HDACis, if we look at it from a structural biology perspective. So, looking at the pose of TSA in the co-crystallized structure with the human HDAC8 (PDB ID: 1T64) and considering that hydroxamic acid group chelates the zinc ion in a bidentate fashion and forms hydrogen bonds with Tyr306 and Asp178 (Fig. 2B) we designed, as new ZBGs, a (2-formylhydrazinylidene)methyl (a), a [2-(trifluoroacetyl)hydrazinylidene]methyl (b), a (2-formylhydrazinyl)carbonyl (c), and a (trifluoroacetyl)carbamoyl (d) moieties (Fig. 2A) which could coordinate the zinc ion bi- or tridentately and could also form hydrogen bonds with Tyr306, Asp178, and, probably, with other amino acids at the bottom of the channel (Fig. 2B). Contemporarily, we choose as linker a *para* disubstituted benzene carrying in *ortho* to ZBG a hydroxyl functionality that, in principle, could be further involved in the zinc chelation. Finally, for the CAP we focused on the bifenilsulfonamide basing on an extensive

QSAR modeling study of sulfonamide HDACis [23]. The new four molecules **1a**–**d** have been represented in Figure 2A.

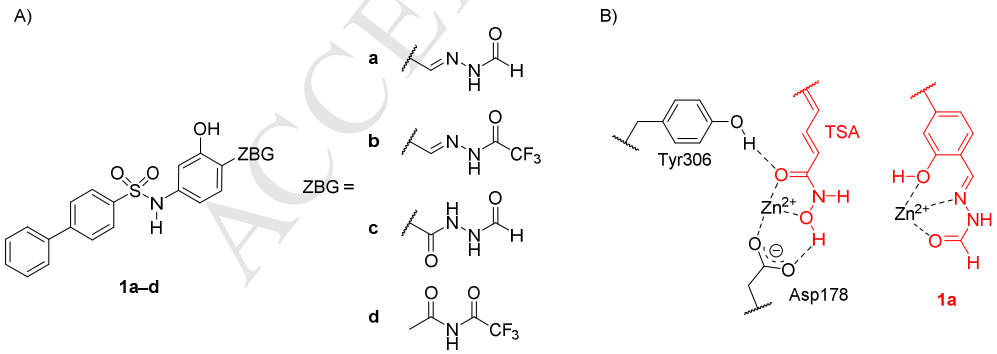

Fig. 2. A) Chemical structure of the new designed potential HDACis **1a**–**d**. B) Interactions of TSA in the co-crystallized structure with the human HDAC8 (PDB ID: 1T64) and proposed tridentate chelation of the ZBG of **1a** with Zn^{2+}.

In paragraph 2.3.1. lines 7 and 9 please substitute:

"The transcribed proteins, analyzed by a Western blot assay as described in material and method …"

with

"The transcribed proteins, analyzed by an immunofluorescence assay as described in material and method …"

and

"Consistently, Western blot analysis revealed that TSA alone, …"

with

"Consistently, the immunofluorescence analysis revealed that TSA alone, …"